A Smart Electrostatic Sensor for On-line Condition Monitoring of Power Transmission Belts

Yonghui Hu, Shuai Zhang, Yong Yan, *Fellow, IEEE*, Lijuan Wang, Xiangchen Qian, and Lu Yang

Abstract — On-line condition monitoring of power transmission belts is essential to keep industrial belt-driven equipment functioning smoothly and reliably. This paper presents a smart electrostatic sensor that monitors belt motion through detection of static charge on the belt. A theoretical model is established using the method of moments for calculation of induced charge on strip-shaped electrodes placed in the vicinity of a belt moving both axially and transversely. The sensor unit converts the induced charge into proportional voltage signals using charge amplifiers and measures belt speed and vibration through cross correlation and spectral analysis, respectively. The performance of the smart electrostatic sensor is validated against a photoelectric rotary encoder and a laser displacement sensor. Comparative experimental results show that the belt speed can be measured with a relative error within $\pm 2\%$ over the range 1.7-15.5 m/s. The electrostatic sensor is capable of measuring the frequencies of transverse vibration accurately. Although absolute displacement cannot be measured due to the uncertain level of charge on the belt, the measurement results of relative vibration magnitudes for different modes and at different belt speeds are reasonably accurate.

Index Terms—Static charge, power transmission belt, smart electrostatic sensor, speed measurement, vibration measurement.

I. INTRODUCTION

THE electrification of dielectric materials due to physical contact, friction and collision is an ubiquitous phenomenon in both nature and industry. Although the discharge of static electricity has caused countless accidents and catastrophes such as fire, explosion and failure of electronic components, the electrostatic charge, if detected using suitable instruments, can provide useful information on machine condition and process characteristics. By making good use of this phenomenon, a variety of monitoring and diagnostic objectives have been achieved. For instance, the measurement of gas-solid two-phase flow in pneumatic conveying pipelines [1, 2] and fluidized beds [3, 4] has been achieved by monitoring the electrostatic noise induced on metal electrodes due to the flow of charged particles. The electrostatic detection of debris in

Y. Hu, S. Zhang, L. Wang, X. Qian, and L. Yang are with the School of Control and Computer Engineering, North China Electric Power University, Beijing 102206, China. (e-mail: huyhui@gmail.com; zhangshuaixufeng@163.com; wwlljj2007@126.com; xcqian@live.com; yanglu910715@126.com)

Y. Yan is with the School of Engineering and Digital Arts, University of Kent, Canterbury CT2 7NT, U.K. (e-mail: y.yan@kent.ac.uk).

exhaust gas was investigated by Addabbo *et al.* [5] and Wen *et al.* [6] for the health monitoring of aero-engines. Noras *et al.* [7] explored the use of a quasi-electrostatic field sensor array for detection of a moving charged bullet. Yawootti *et al.* [8] developed an electrostatic PM10 mass monitor for continuous measurement of ambient particulate air pollution. In addition, wear detection of a taper roller bearing was studied by Harvey *et al.* [9] using an electrostatic condition monitoring system. With a growing realization of the ubiquity and role of the electrostatic charge in various natural and industrial processes, the electrostatic monitoring technique is finding applications in an increasingly wide variety of fields.

Recently, preliminary studies have been carried out on speed and vibration measurement of power transmission belts using electrostatic sensors [10, 11]. Belt drives are extensively used in many industries to transmit torque between rotating shafts. On-line condition monitoring of power transmission belts plays an essential part in detecting wear, misalignment, improper tensioning and other incipient mechanical defects, hence preventing performance degradation and unscheduled downtime. A dielectric belt can become electrically charged due to its contact and friction with the roller and the air. The combined axial and transverse motion of the belt creates a fluctuating electric field and generates an induced current signal on a metal electrode placed in the vicinity of the belt. The axial speed of the belt was determined by cross correlating the signals from upstream and downstream sensors, whilst the belt transverse velocity was characterized through the Fourier analysis of the signals. Non-contact measurement of belt speed and vibration is a difficult problem with only a few practical solutions available, among which the laser Doppler velocimeter [12] and vibrometer [13] are regarded as the most effective. In comparison with laser-based instruments that are complex, delicate and expensive, the electrostatic sensor is simple, cost-effective, well-suited for a dusty environment and capable of simultaneous speed and vibration measurement, thus offering great potential for routine industrial applications.

In the present study, a smart electrostatic sensor that incorporates functions of charge detection, signal conditioning, data processing and communication for on-line belt condition monitoring was developed and experimentally assessed. The correlation between the sensor response and the belt kinematics is established through theoretical modelling and numerical simulation. Based on the simulation results, algorithms for measuring belt speed and vibration are designed and implemented using the on-board microcontroller. The measurement results of the smart electrostatic sensor are validated against two well-established measurement techniques. Meanwhile, exten-

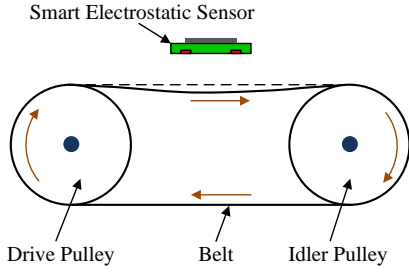Fig. 1. Measurement principle of the smart electrostatic sensor.

Fig. 2. Coordinate system for modelling of the electrostatic sensor.

sive experimental investigations were carried out to assess its performance under different conditions on a purpose-built test rig.

The smart electrostatic sensor is in effect a highly-integrated measurement system capable of non-contact sensing of static charge and translating sensor data into meaningful measurements through embedded computing. The compact, non-contact design reduces noise from wiring and offers great flexibility and ease of deployment in various applications. It automatically adjusts the sensitivity to changes in charge level on the belt. In addition, the communication link of USB 2.0 bus offers a fast data transfer rate for both the complete raw signals and measurement results, allowing the user to examine the belt condition in great detail.

II. THEORETICAL ANALYSIS AND NUMERICAL SIMULATION

A. Measurement Principle

The smart electrostatic sensor features two strip-shaped electrodes and charge amplifiers for the detection of static charges on the belt. During operation, the power transmission belt undergoes a combined axial and transverse motion, exhibiting a travelling wave along the belt length. The cyclic movement of approaching and moving away of the belt relative to the electrodes leads to variation of the induced charge on the electrodes. By converting the induced charge into voltage signals using charge amplifiers, information about the belt transverse displacement can be derived. The two electrodes placed in parallel in the belt running direction experience different phases of the belt travelling wave. By exploiting the spatial phase shift in the signals, the belt axial speed is determined. Fig. 1 illustrates the measurement principle of the smart electrostatic sensor.

B. Induced Charge on the Electrodes

In order to elucidate how the electrostatic sensor responds to the motion of the belt, the amount of induced charge on the electrodes is calculated. The uniformity of charge distribution on the belt is mainly affected by the surface roughness. For a smooth, unworn and uncontaminated belt, it is reasonable to assume uniform charge distribution on the belt. According to the superposition principle of electrostatic fields, the total induced charge on the electrode is due to all charges on the belt. Consequently, for the sake of simplicity, a single point charge that moves along the belt trajectory is used in the analysis.

In previous modelling work of electrostatic sensors [5, 14, 15], the method of image charges was used to calculate the electrical potential at any point in space and the surface charge
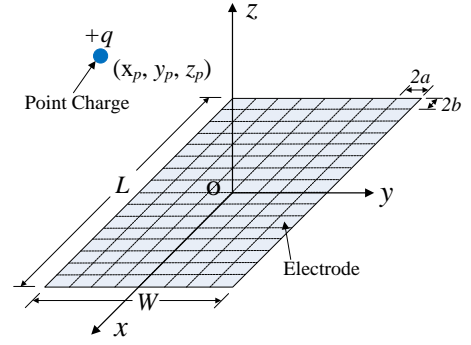
density on the electrode. However, the validity of this method rests upon the condition that the conducting plane is of infinite extent and depth. As has been reported in [16], the errors incurred when solving electrostatic problems involving finite conducting planes (such as the electrode) can be significant, especially when the point charge is located far away from the plane. Therefore, a more accurate method, i.e. the method of moments is used in this study to determine the surface charge distribution induced on the electrodes by the point charge [17].

Assume the electric crosstalk between the electrodes and the influence of nearby conductors are negligible, then the potential distribution around an electrode is only due to the point charge and the induced charge on the electrode. Consider an electrode lying on the xoy-plane and centered at the origin of a local coordinate system shown in Fig. 2. The length and width of the electrode is L and W, respectively, while its thickness is assumed to be zero. A point charge $+q$ is located at some position (x_p, y_p, z_p) above the electrode. Then according to Coulomb's law and the superposition principle of electrostatic fields [18], the potential at an arbitrary observation point (x, y, z) is evaluated as

$$V(x,y,z) = \int_{-\frac{W}{2}}^{\frac{W}{2}} \int_{-\frac{L}{2}}^{\frac{L}{2}} \frac{\rho(x',y')dx'dy'}{4\pi\varepsilon\sqrt{(x-x')^2+(y-y')^2+(z-z')^2}} + \frac{q}{4\pi\varepsilon\sqrt{(x-x_p)^2+(y-y_p)^2+(z-z_p)^2}} \quad (1)$$

where ε is the permittivity of the medium, (x', y', z') denotes the coordinate of the induced charge on the electrode, and $\rho(x', y')$ represents the surface charge density, which is to be determined. Employing the method of moments, the electrode is divided into $N \times M$ small sections of equal area, where N and M are the numbers of sections along the length and width directions, respectively. These sections are sufficiently small so that the charge distribution in each section can be assumed to be uniform. Then equation (1) reduces to

$$V(x,y,z) = \sum_{i=1}^{N \times M} \int_{y_{ci}-a}^{y_{ci}+a} \int_{x_{ci}-b}^{x_{ci}+b} \frac{\rho_i dx'dy'}{4\pi\varepsilon\sqrt{(x-x')^2+(y-y')^2+(z-z')^2}}$$
$$+ \frac{q}{4\pi\varepsilon\sqrt{(x-x_p)^2+(y-y_p)^2+(z-z_p)^2}}, \ i=1, 2, ..., N \times M$$

$$(2)$$

where $a = \dfrac{W}{2M}$, $b = \dfrac{L}{2N}$, ρ_i is the surface charge density and (x_{ci}, y_{ci}, z_{ci}) the coordinate of the center of the i-th section. In order to determine the unknown values of ρ_i in equation (2), a total of $N \times M$ equations are required. Since the potential of the electrode is known, the desired $N \times M$ equations are obtained by evaluating the potential at the center of each section, which is the same as the electrode potential. Hence,

$$V_j = \sum_{i=1}^{N \times M} \int_{y_{ci}-a}^{y_{ci}+a} \int_{x_{ci}-b}^{x_{ci}+b} \frac{\rho_i dx' dy'}{4\pi\varepsilon\sqrt{(x_{cj}-x')^2+(y_{cj}-y')^2}}$$

$$+ \frac{q}{4\pi\varepsilon\sqrt{(x_{cj}-x_p)^2+(y_{cj}-y_p)^2+(z_{cj}-z_p)^2}}, \quad j=1,\ 2,\ ...,\ N \times M \tag{3}$$

where V_j is the potential at the center of the j-th section. Equation (3) can also be written as

$$V_j = \sum_{i=1}^{N \times M} \rho_i V_{ji} + \frac{q}{4\pi\varepsilon\sqrt{(x_{cj}-x_p)^2+(y_{cj}-y_p)^2+(z_{cj}-z_p)^2}} \tag{4}$$

where V_{ji} is the potential at the center of the j-th section due to unit charge density in the i-th section.

For $i = j$, the potential at the center of each section because of its own charge is calculated as

$$V_{ji} = \int_{y_{ci}-a}^{y_{ci}+a} \int_{x_{ci}-b}^{x_{ci}+b} \frac{dx'dy'}{4\pi\varepsilon\sqrt{(x_{ci}-x')^2+(y_{ci}-y')^2}}$$

$$= \frac{1}{\pi\varepsilon}\left[aIn(\frac{\sqrt{a^2+b^2}+b}{a}) + bIn(\frac{\sqrt{a^2+b^2}+a}{b})\right] \tag{5}$$

For $i \neq j$, treating the charge in the i-th section as a point charge located at the center leads to

$$V_{ji} = \frac{ab}{\pi\varepsilon\sqrt{(x_{cj}-x_{ci})^2+(y_{cj}-y_{ci})^2}} \tag{6}$$

After computing all V_{ji}, the $N \times M$ equations represented by equation (4) are solved through simple matrix algebra routines to obtain a discrete approximation of the surface charge density. Then the total induced charge q' on the electrode is determined from

$$q' = \sum_{i=1}^{N \times M} 4\rho_i ab \tag{7}$$

C. Output Voltage of the Charge Amplifiers

The induced charge on the electrodes is measured via charge amplifiers. In most previous research involving electrostatic sensors, transresistance amplifiers (i.e., current-to-voltage converters) were used for signal conditioning. By measuring the rate of variation in the induced charge (i.e., the induced current), the transverse velocity of the belt vibration was characterized [10, 11]. By contrast, charge amplifiers can deliver displacement response, which will be verified through numerical simulation and comparative experiments.

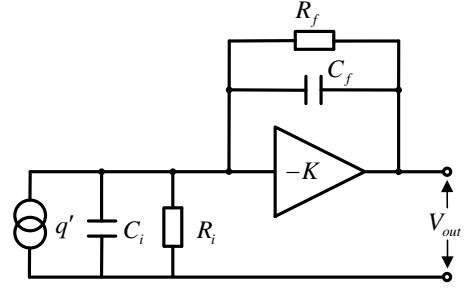Fig. 3 shows an equivalent circuit of the electrode and the

Fig. 3. Equivalent circuit of the electrode and the charge amplifier.

charge amplifier. The electrode is modelled as a charge source that delivers or accepts electrons depending on the variation of the induced charge. The charge amplifier integrates the input charge on a feedback capacitor C_f connected across an inverting amplifier with an open-loop voltage gain of $-K$. To prevent the charge amplifier from drifting into saturation due to the leakage current at the amplifier input, a large-value resistor R_f that continuously bleeds off the accumulated charge is placed in parallel with C_f. The capacitance C_i is the sum of the electrode capacitance and the input capacitance of the operational amplifier, while the resistance R_i represents the total insulation resistance at the input.

From the equivalent circuit in Fig. 3, the output voltage V_{out} of the charge amplifier is expressed as

$$V_{out} = -\frac{q'}{(1+\frac{1}{K})(C_f + \frac{1}{j\omega R_f}) + \frac{1}{K}(C_i + \frac{1}{j\omega R_i})} \tag{8}$$

At low frequencies, an operational amplifier has a very high and approximately constant open-loop gain, which rolls off at the rate of -20 dB/dec at higher frequencies [19]. It has been illustrated by experiments (see Section IV) that the frequency of the electrostatic signal collected around the belt is very low (approximately 100 Hz at the highest belt axial speed). Therefore, for a very large open-loop gain ($K > 10^5$), equation (8) can be simplified into

$$V_{out} = -\frac{q'}{C_f + \frac{1}{j\omega R_f}} \tag{9}$$

As can be seen from equation (9), the effect of the input capacitance and resistance on the output voltage is negligible at low frequencies. It is also noticeable that the feedback capacitor and resistor form a RC-high-pass filter [20], suggesting that the integrating behavior at low frequencies is suppressed by R_f. The cut-off frequency of the filter is given by
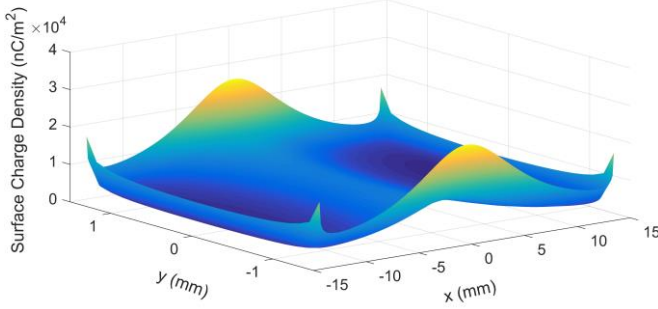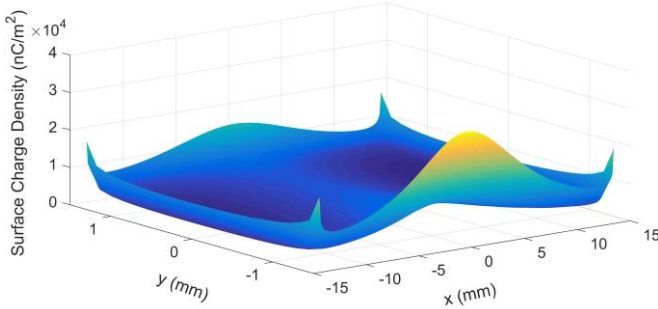
$$f_c = \frac{1}{2\pi R_f C_f} \tag{10}$$

In order to improve the low-frequency response, the feedback resistor should be sufficiently large. In an ideal case with infinitely large feedback resistor, equation (9) can be further reduced to
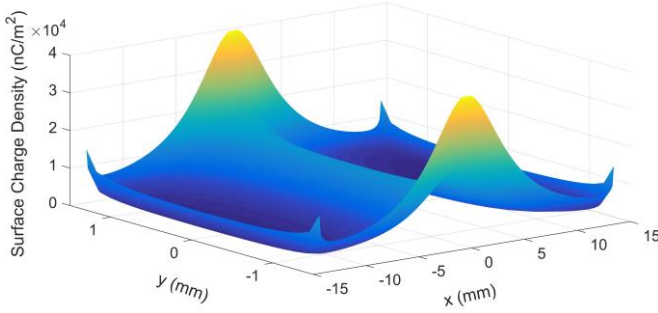
(a) Position of the point charge: (0, 0, 4).

(b) Position of the point charge: (0, 0, 6).

(c) Position of the point charge: (0, -4, 6).

Fig. 4. Surface charge density for different positions of the point charge.

$$V_{out} = -\frac{q'}{C_f} \qquad (11)$$

It is evident that the output voltage is directly proportional to the induced charge on the electrode and the charge sensitivity of the electrostatic sensor can be controlled via the feedback capacitor.

D. Numerical Simulation

The surface charge density and the total induced charge on the electrode due to a point charge are computed numerically. The length and width of the electrode are 28 mm and 3 mm, respectively, and the numbers of sections along the length and width directions are 224 and 24, respectively. The relative permittivity of the medium, namely the air is 1.0. The potential of the electrode is set as zero. Fig. 4 shows the surface charge density when a -1 nC negative point charge is placed at different positions. As can be seen, the negative point charge induces positive charges on the electrode. Due to the edge effect, the surface charge density increases considerably near
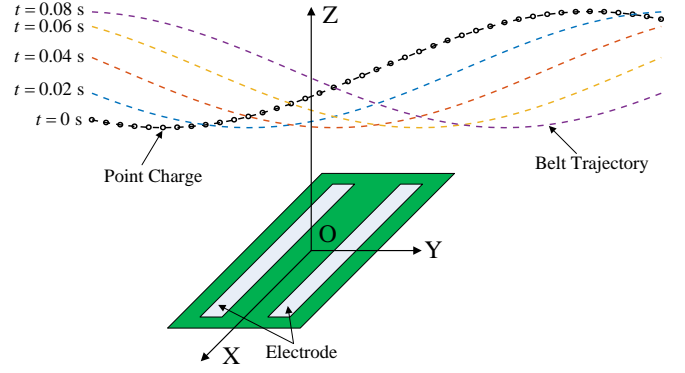

Fig. 5. Schematic diagram of the simulation setup.

corners and edges, especially at edge points closest to the point charge. When the point charge is moved further away from the electrode, the total induced charge decreases from 0.554 nC in Fig. 4(a) to 0.456 nC in Fig. 4(b). The deviation of the point charge from the xoz-plane leads to asymmetric charge distribution, as shown in Fig. 4(c).

In order to simulate the response of the electrostatic sensor to the motion of the belt, a global coordinate system is defined, as shown in Fig. 5. The Y-axis of the coordinate system points towards the belt axial direction, the Z-axis points towards the transverse direction and the origin is located at the midpoint between the two electrodes. The dynamics of belt vibration is rather complex, which has received considerable research efforts for decades [21-25]. For simplicity, the combined axial and transverse motion can be viewed as a travelling wave [25]. Taking only the first vibration mode into consideration, the transverse displacement $z(y,t)$ of the belt at spatial coordinate y and time t is described as

$$z(y,t) = B + A\sin(ky - 2\pi ft) \qquad (12)$$

where B denotes the distance between the electrodes and the belt equilibrium position, A represents the amplitude of the wave, k is the wavenumber and f is the vibration frequency. In the simulation, the above parameters are set as follows: $B = 6$ mm, $A = 2$ mm, $k = \pi/100$ and $f = 5$ Hz. The trajectories obtained with these parameters at different time instants are illustrated in Fig. 5. With the assumption of uniform charge distribution on the belt, a series of point charges evenly distributed along the belt trajectory is used to simulate the continuous charge distribution on the belt. The total induced charge on the electrode is then computed as the sum of induced charge from all point charges. Since the induced charge due to faraway point charges is negligible, only point charges within the abscissa range from -50 mm to 50 mm are taken into account. The distance between adjacent point charges along the Y-axis is 1 mm, which follows that a total of 101 point charges is used in the simulation. An increased number of point charges within the specified range leads to enhanced accuracy and more smooth variation of the total induced charge, but the computational cost will also increases significantly. In addition, the spacing between the electrodes is 16 mm.
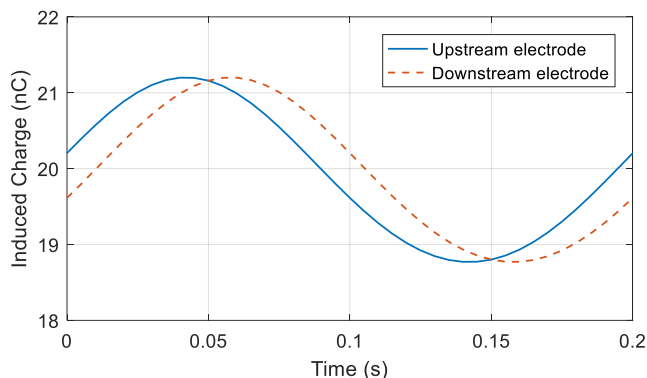
Fig. 6 Induced charge within a period of the travelling wave.

Fig. 6 shows the induced charge on the electrodes within a period of the travelling wave. It can be seen that as the troughs and peaks pass the electrode alternately, the induced charge decreases and increases accordingly, giving rise to a fluctuating charge signal with the same frequency as the vibration. The spatial propagation of the travelling wave and the spacing of the electrodes lead to a time delay between the charge signals, which is exactly the transit time taken by the belt to pass the two electrodes. The above simulation results provide fundamental insights into the generation of the electrostatic signal and shed light on the design of the measurement algorithms to be presented in Section III.

III. DESIGN AND IMPLEMENTATION OF THE SMART ELECTROSTATIC SENSOR

A. Overview

The smart electrostatic sensor is a complete measurement system that combines sensing and processing capabilities for on-line condition monitoring of power transmission belts. Fig. 7 shows a functional block diagram of the sensor unit. The two electrodes, acting as the sensing elements, generate induced charge in response to the motion of the belt. The signal conditioning circuit converts the induced charge into proportional voltage signals at a suitable level for A/D conversion. The embedded intelligence, realized with an on-board microcontroller, provides functionalities related to signal processing, gain adjustment and communication with a host computer. In addition, the sensor unit is powered by an external power supply, which is regulated and filtered to supply the analog and digital circuits separately.

B. Hardware Design

Fig. 8 illustrates the prototype of the sensor unit realized on a four-layer printed circuit board (PCB). The electrodes are fabricated as two long pads on the bottom side, which are shielded from external electromagnetic noise by the surrounding copper fill and internal power planes. The conditioning circuit on the top side is also protected by the internal planes from the influence of the charge on the belt. The charge amplifier uses a LMP7721 operational amplifier with ultra-low input bias current and a feedback capacitor (COG material) of high stability for precision measurement of the induced charge. The value of
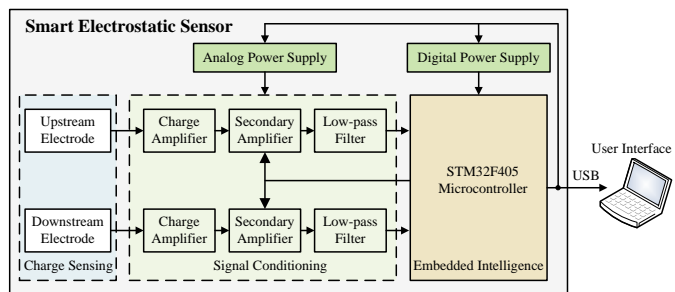

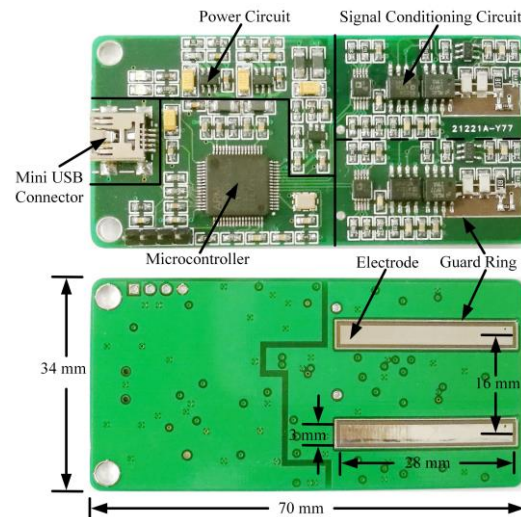Fig. 7. Functional block diagram of the smart electrostatic sensor.

Fig. 8. Photograph of the sensor prototype.

the feedback capacitor is 1 nF, resulting in a charge sensitivity of 1 mV/pC. The feedback resistance that removes the DC component of the electrostatic signal is 1 GΩ, therefore the lower frequency limit of the charge amplifier is 0.16 Hz, which is well below the belt vibration frequency. To minimize the leakage current from the surface of the PCB, the electrode and the non-inverting input terminal of the operational amplifier are protected by guard rings, which are driven to the same potential as the electrode by a voltage follower realized with a LMP7715 operational amplifier. Since the amount of charge carried by the belt depends on a variety of factors such as pulley speed, temperature and atmospheric humidity [26], a secondary amplifier stage that allows gain adjustment and brings the signal to a level suitable for subsequent A/D conversion is implemented using an AD8602 operational amplifier and a 4-channel analog multiplexer ADG704. The electrostatic signal is then filtered by a Salley-Key low-pass filter with a cut-off frequency of 2 kHz.

The electrostatic signals are sampled and processed by a STMicroelectronics STM32F405 microcontroller that features an ARM Cortex-M4 core running at 168 MHz, 192 Kbyte of SRAM, 1 Mbyte of Flash memory and 12-bit A/D converters. The microcontroller provides sufficient computing resources for real-time signal processing and data analysis. The sensor unit communicates with the host computer via a USB 2.0 bus. Both the raw electrostatic signals and the measurement results are transmitted and presented to the user. The power of the sensor is supplied directly through the USB cable, thus eliminating the need for a separate power supply. Two TPS79301

low-dropout linear regulators are used to step down the input +5 V voltage to +3.3 V to power the signal conditioning circuit and the microcontroller. The final, fully assembled smart electrostatic sensor as shown in Fig. 8 is of small form factor, low power consumption and low cost, thus enabling easy and rapid deployment in various industrial applications.

C. Measurement Algorithm and Software Design

As discussed above, the time delay between the upstream and downstream signals corresponds to the transit time taken by the belt to pass the two electrodes. Therefore, the belt axial speed can be measured by exploiting the similarity and time delay between the signals. Cross-correlation is a common signal processing technique that measures the similarity of two signals as a function of time shift [1, 2, 3, 10, 11, 14, 27, 28]. It involves progressively sliding of one signal past the other and summing the cross-multiplication products over the common time interval. The normalized cross-correlation function defined as follows reaches a dominant peak at the time delay τ when the two signals are best aligned

$$R(m) = \frac{\sum_{i=1}^{I} s_u(i) s_d(i+m)}{\sqrt{\sum_{i=1}^{I} s_u^2(i)} \sqrt{\sum_{i=1}^{I} s_d^2(i)}} \qquad (13)$$

where $s_u(i)$ and $s_d(i)$ represent the discretized, zero mean signals from the upstream and downstream sensors, respectively, I is the number of samples and m ($m = 0, 1, ..., I$) is the number of delayed points. After locating the dominant peak in the normalized cross-correlation function and using the spacing D between the two electrodes, the belt axial speed is calculated from

$$v = \frac{D}{\tau} \qquad (14)$$

In addition, the value of the dominant peak, called correlation coefficient, reflects the similarity of the two signals.

From the aforementioned measurement principle, it can be seen that the electrostatic sensor is essentially a proximity probe capable of non-contact measurement of dynamic displacement. Although the absolute displacement cannot be measured due to the uncertain amount of charge on the belt, the transverse vibration can still be quantitatively characterized through identification of the vibration modes and their relative magnitudes. In this study, the traditional vibration analysis method, i.e. spectral analysis via Fourier transform is applied. The Cooley–Tukey algorithm of the fast Fourier transform (FFT) is implemented on the microcontroller to generate a spectrum that includes all of the signal's constituent frequencies. To enhance the reliability of the measurement results, the amplitude spectra of the two signals are fused as follows

$$S(\omega) = \frac{|S_u(\omega)| + |S_d(\omega)|}{2} \qquad (15)$$

where $S_u(\omega)$ and $S_d(\omega)$ represent the Fourier spectra of the upstream and downstream signals, respectively. Then the spectral peaks that correspond to vibration modes and provide important information for fault diagnosis are detected.

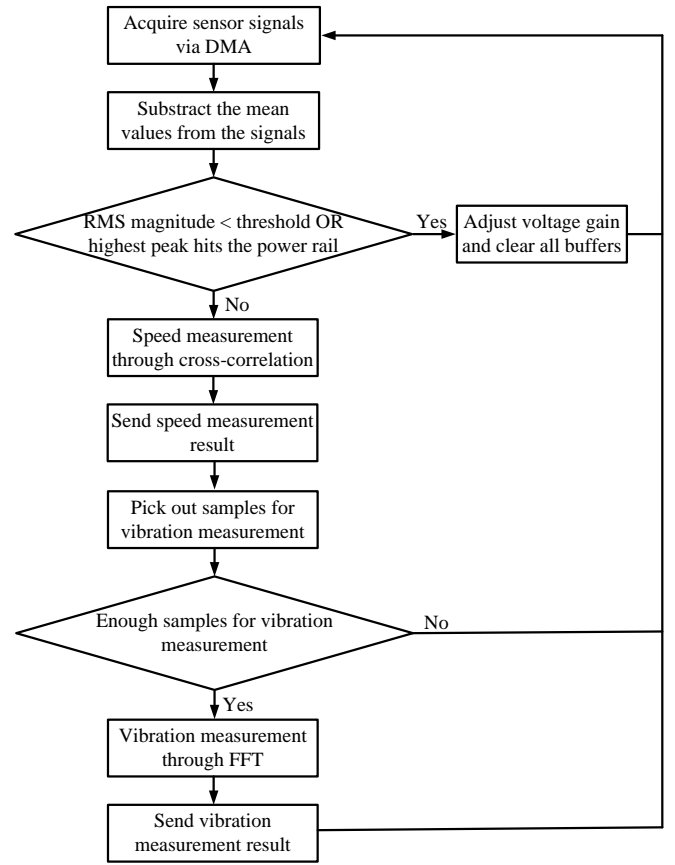As can be seen from Equation (14), the measurement accu-

Fig. 9. Flowchart of the embedded software.

racy of the belt speed depends strongly on the error of the time delay which is in the order of a few milliseconds. In order to determine the time delay accurately, a higher sampling rate that leads to a closer discrete approximation of the true time delay is desirable [27, 28]. On the other hand, the accurate determination of the vibration frequency requires a long sampling time, which equals the reciprocal of the frequency resolution. These requirements pose high demands on the memory and computing power, which are very limited on the microcontroller. The strategy employed to solve this problem is to perform speed and vibration measurements using different sample sets. The signals are sampled at 50 kHz for a period of 0.2 s and stored in a ping-pong buffer (actually two separate buffers filled and processed alternately) for speed measurement. For vibration measurement, one for every 50 samples is picked out and stored in another ping-pong buffer, resulting in a sampling rate of 1 kHz. The FFT algorithm is executed when a total of 4096 samples are acquired, which follows that the frequency resolution of vibration measurement is about 0.25 Hz.

The software embedded in the microcontroller consists of a series of functional modules executed sequentially in an infinite loop. Fig. 9 is a flowchart illustrating the main steps of the measurement process. The ADC samples are transferred to the ping-pong buffer for speed measurement via DMA, while the samples for vibration measurement are picked out by the software. Although the charge amplifier is discharged continuously by the feedback resistor to remove the DC component, the non-stationary vibration of the belt and the offset errors of
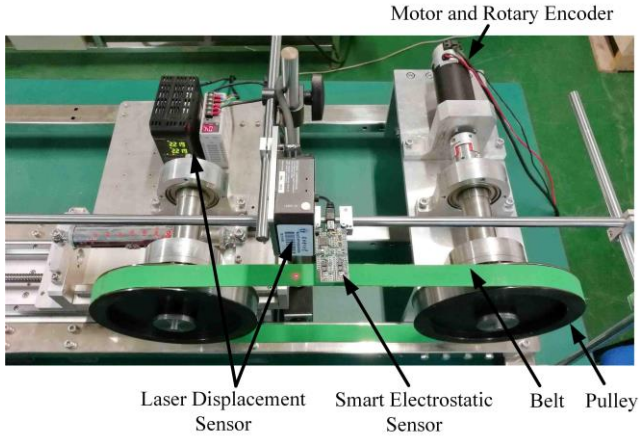
Fig. 10. Experimental setup.

Fig. 11. Electrostatic signals and transverse displacement when the belt axial speed is 6.18 m/s.

the operational amplifier still introduce an offset voltage. Therefore, the electrostatic signals are zero-meaned by the software as the first step of processing. In view of the variable charge level on the belt, the root-mean-square (RMS) magnitude of the electrostatic signal is computed and the highest voltage peak that indicates potential saturation is identified for adjustment of the voltage gain of the secondary amplifier stage. Then the belt speed is calculated for each iteration of the loop, and only when enough samples have been acquired the vibration is measured. Once available, the result of a measurement is sent to the host computer by a communication subroutine.

IV. EXPERIMENTAL EVALUATION

A. Experimental Setup

The smart electrostatic sensor was experimentally assessed on a purpose-built test rig, as shown in Fig. 10. The belt to be measured is a flat, nylon-type belt stretched over two pulleys of an equal diameter of 0.2 m. One of the pulleys is driven by a DC motor. The axial speed of the belt is adjusted by regulating the voltage applied to the DC motor, while the vibration is naturally generated without any external forcing. The smart electrostatic sensor is mounted above the belt on a supporting frame.

The performance of the smart electrostatic sensor was validated against two well-established reference sensors. An incremental photoelectric rotary encoder with 1000 pulses per revolution measures the rotational speed of the DC motor. Under the condition of proper tensioning and no slip between the belt and pulleys, the belt axial speed can be easily calculated from the rotational speed. A separate microcontroller-based circuit board counts the pulse from the encoder and delivers the belt axial speed. The reference sensor for vibration measurement is a laser displacement sensor (controller model LK-G5001 and sensor head model LK-H085, Keyence CO., Ltd.) that measures its distance to the belt with high accuracy. The analog output of the laser displacement sensor is sampled at a frequency of 50 kHz using a National Instruments DAQ device (model USB-6363) and converted proportionally into displacement.
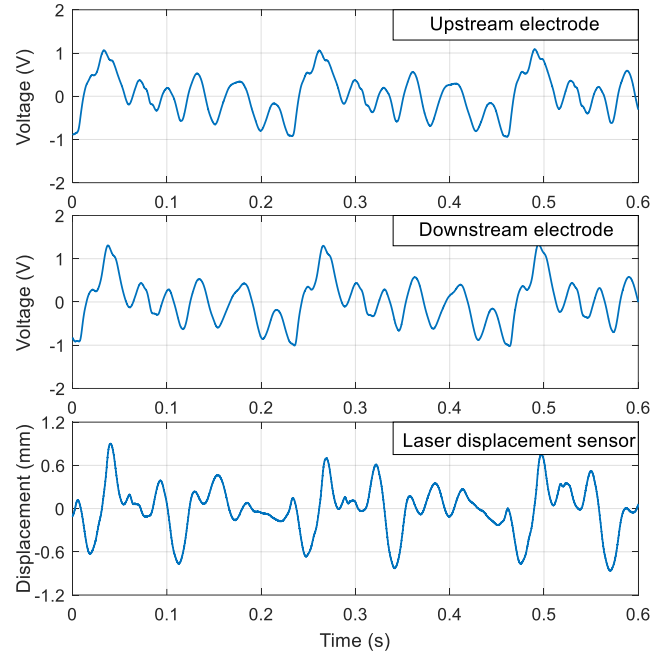
B. Experimental Results

Fig. 11 shows the electrostatic signals and transverse displacement when the belt axial speed measured with the rotary encoder is 6.18 m/s and the distance between the electrostatic sensor and the equilibrium position of the belt is 20 mm. As can be seen, the two electrostatic signals have very similar waveforms and a short time delay between them is clearly observable. By computing the normalized cross-correlation function illustrated in Fig. 12, the time delay is determined as 2.62 ms, which gives a speed measurement of 6.11 m/s. The small relative error of -1.13% and a correlation coefficient as high as 0.97 can therefore validate the effectiveness of the electrostatic sensor for belt speed measurement.

The belt vibrates with a peak-to-peak displacement of 1.5 mm, as shown in Fig. 11. Due to the different sensing mechanisms, the similarity between the electrostatic signals and the waveform of transverse displacement is not so evident. In order to quantify the similarity, the downstream electrostatic signal and the transverse displacement are normalized with respect to their own peak magnitudes and then cross correlated. A correlation coefficient of 0.56 is obtained, suggesting that the two measurements are strongly related to each other. In addition, the amplitude spectra of the electrostatic signals and the transverse displacement are computed and plotted in Fig. 13. It can be seen that the amplitude spectra of the up-stream and downstream signals are nearly identical and there exist strong, well-separated spectral peaks at the fundamental and harmonic frequencies in both the electrostatic and dis-placement measurements. Such a spectral pattern, which is typical of mechanical vibrations, and the close agreement between the spectra of both measurements verify that the variation of induced charge and hence the electrostatic signals are mainly attributed to the belt vibration. The fundamental vibration frequency is exactly
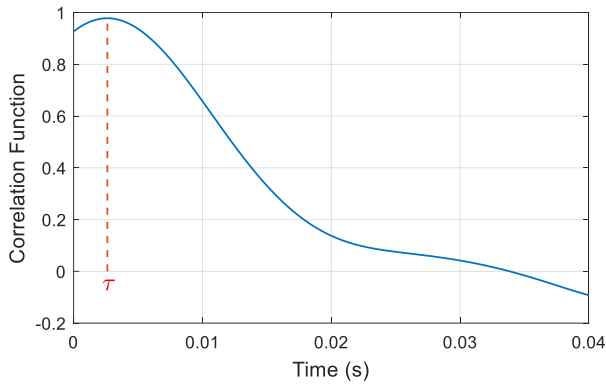
Fig. 12. Normalized cross-correlation function between upstream and downstream electrostatic signals.
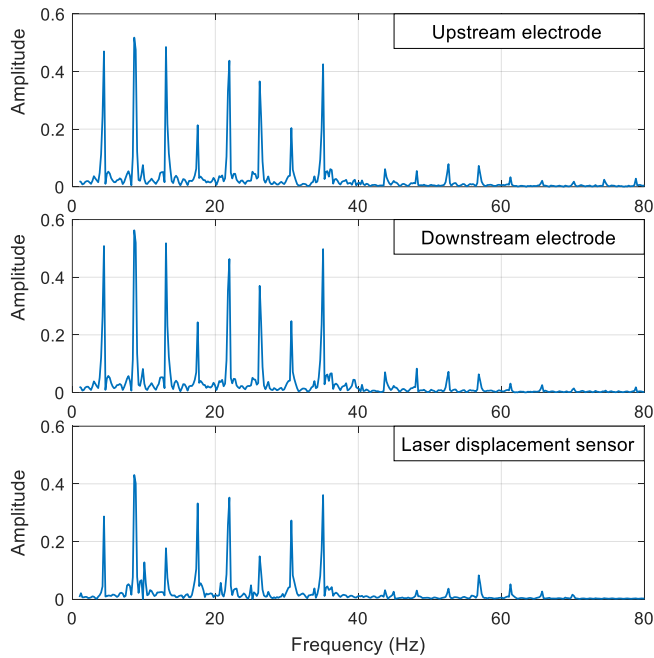

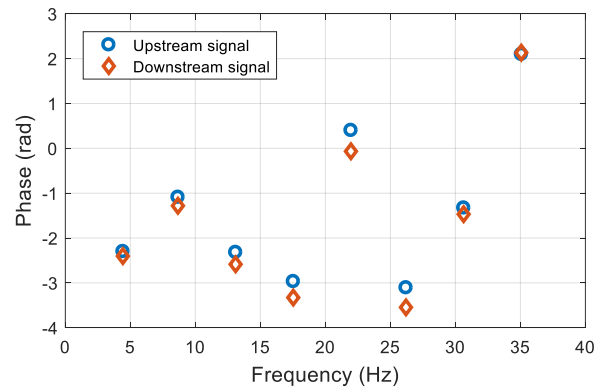Fig. 13. Amplitude spectra of the electrostatic signals and transverse displacement.

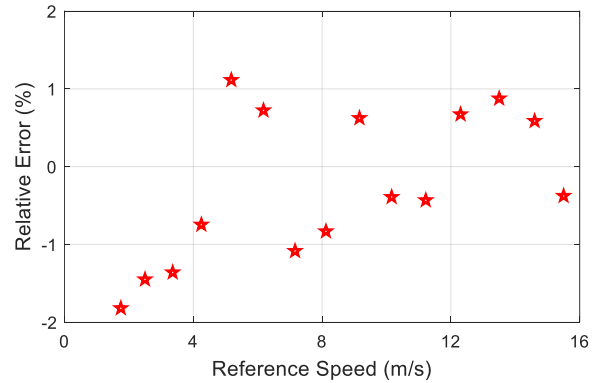Fig. 14. Phase angles of the electrostatic signals at the vibration frequencies.
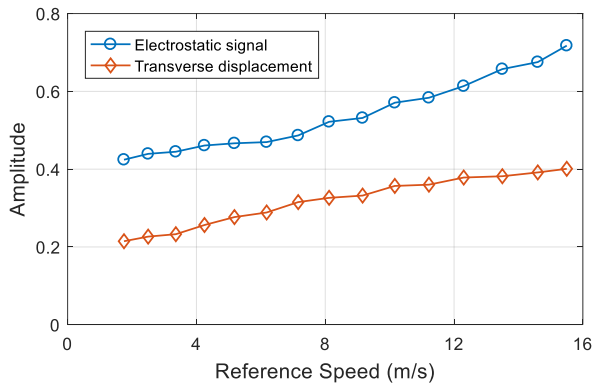

Fig. 15. Relative error of the measured speed.

Fig. 16. Amplitudes of the first vibration mode at different speeds.

the belt transport frequency, which is defined as the belt axial speed divided by the belt length (1.4 m). The electrostatic sensor can identify the vibration frequencies accurately. In general, the relative magnitudes of the spectral peaks in both measurements agree well with each other, although there exist slight discrepancies due to the different sensing mechanisms.

To better understand the underlying principle of speed measurement, the phase angles of the electrostatic signals at the vibration frequencies are plotted in Fig. 14. As can be seen, there exist phase lags between the upstream and downstream signals at all vibration frequencies. It can thus be confirmed that the spatial phase shift experienced by the two electrodes gives rise to the time delay between the signals, which contains the speed information.

The accuracy of the smart electrostatic sensor for belt speed measurement was assessed by varying the speed from 1.7 to 15.5 m/s. Fig. 15 depicts the relative error of the measured speed, which is the averaged value of 50 measurements with normalized standard deviation less than 1%. As illustrated, the

relative error is within ±2% throughout the speed range. At a lower speed, typically below 5.0 m/s, the relative error decreases with the belt speed because of the increasingly intensive belt vibration and clearer phase shift between the upstream and downstream signals. For a belt speed higher than 5 m/s, the relative error shows no apparent dependence on the speed.

Throughout the range of tested speed, the electrostatic signals and transverse displacement have amplitude spectra similar to those shown in Fig. 13. The vibration frequencies increase linearly with the belt speed, while the amplitudes of the first vibration mode at different belt speeds are shown in Fig. 16. It is shown that the increased speed leads to higher amplitudes of both measurements. The amplitude of the electrostatic signal increases more rapidly than that of the displacement meas-

urement, which is attributed to the increased charge level on the belt at a higher speed.

V. CONCLUSIONS AND FUTURE WORK

In this paper, a smart electrostatic sensor working on the principle of static charge detection has been designed and implemented to measure the axial speed and transverse vibration of a power transmission belt. Theoretical modeling and numerical simulation have been conducted to establish the relationship between the sensor response and the belt kinematics. The design and implementation of the hardware, software and measurement algorithms have been presented. The performance of the smart electrostatic sensor has been assessed with reference to a photoelectric rotary encoder and a laser displacement sensor. Results obtained have demonstrated that the belt speed can be measured with a relative error within $\pm 2\%$ over the range $1.7-15.5$ m/s. The belt vibration frequencies measured using the electrostatic sensor and the laser displacement sensor are exactly the same, whereas the measurement results of relative vibration levels for different modes and at different belt speeds are reasonably accurate.

In future work, the smart electrostatic sensor will be assessed in real industrial environments under variations in ambient temperature, relative humidity, dust level and electromagnetic noise. The capabilities of the sensor will be further augmented with advanced signal processing algorithms enabling fault detection, self-diagnosis and prognosis.

ACKNOWLEDGMENT

REFERENCES

[1] J. R. Coombes and Y. Yan, "Measurement of velocity and concentration profiles of pneumatically conveyed particles using an electrostatic sensor array," *IEEE Trans. Meas. Instrum.*, vol. 65, no. 5, pp. 1139-1148, 2016.

[2] C. Xu, S. Wang, J. Li and S. Wang, "Electrostatic monitoring of coal velocity and mass flowrate at a power plant," *Instrum. Sci. Technol.*, vol. 44, no. 4, pp. 353-365, 2016.

[3] W. Zhang, Y. Yan, Y. Yang and J. Wang, "Measurement of flow characteristics in a bubbling fluidized bed using electrostatic sensor arrays," *IEEE Trans. Meas. Instrum.*, vol. 65, no. 3, pp. 703-712, 2016.

[4] C. He, X. T. Bi and J. R. Grace, "Comparison of conventional and novel probes for measuring electrostatics and hydrodynamics during fluidization of polyethylene," *J. Electrostat.*, vol. 79, pp. 7-15, 2016.

[5] T. Addabbo, A. Fort, R. Garbin, M. Mugnaini, S. Rocchi and V. Vignoli, "Theoretical characterization of a gas path debris detection monitoring system based on electrostatic sensors and charge amplifiers," *Measurement*, vol. 64, pp. 138-146, 2015.

[6] Z. Wen, H. Zuo and M. G. Pecht, "Electrostatic monitoring of gas path debris for aero-engines," *IEEE Trans. Reliab.*, vol. 60, no. 1, pp. 33-40, 2011.

[7] M. A. Noras, S. P. Ramsey, B. B. Rhoades, "Projectile detection using quasi-electrostatic field sensor array," *J. Electrostat.*, vol. 71, no. 3, pp. 220-223, 2013.

[8] A. Yawootti, P. Intra, N. Tippayawong and S. Sampattagul, "Field evaluation of an electrostatic PM10 mass monitor used for continuous ambient particulate air pollution measurements," *J. Electrostat.*, vol. 78, pp. 46-54, 2015.

[9] T. J. Harvey, R. J. K. Wood, H. E. G. Powrie, "Electrostatic wear monitoring of rolling element bearings," *Wear*, vol. 263, no. 7-12, pp. 1492-1501, 2007.

[10] Y. Hu, Y. Yan, L. Wang, X. Qian and X. Wang, "Simultaneous measurement of belt speed and vibration through electrostatic sensing and data fusion," *IEEE Trans. Instrum. Meas.*, vol. 65, no. 5, pp. 1130-1138, 2015.

[11] Y. Hu, Y. Yan, L. Wang and X. Qian, "Non-contact vibration monitoring of power transmission belts through electrostatic sensing," *IEEE Sens. J.*, vol. 16, no. 10, pp. 3541-3550, 2016.

[12] N. Morita, H. Nogami, E. Higurashi, T. Ito and R. Sawada, "Development of a built-in micro-laser Doppler velocimeter," *J. Microelectromech. Syst.*, vol. 25, no. 2, pp. 380-387, 2016.

[13] P. Chiariotti, M. Martarelli and P. Castellini, "Exploiting continuous scanning laser Doppler vibrometry in timing belt dynamic characterization," *Mech. Syst. Signal Pr.*, in press, published online.

[14] L. Wang and Y. Yan, "Mathematical modelling and experimental validation of electrostatic sensors for rotational speed measurement," *Meas. Sci. Technol.*, vol. 25, p. 115101, 2014.

[15] J. Lin, Z. Chen, Z. Hu, Y. Yang and X. Tang, "Analytical and numerical investigations into hemisphere-shaped electrostatic sensors," *Sensors*, vol. 14, no. 8, pp. 14021-14037, 2014.

[16] R. Nelson, S. Jalil and J. Mu, "Using image theory for finite electrostatic problems - some observations and guidelines," in *Proc. IEEE 1997 Int. Symp. Electromagnetic Compatibility*, Austin, USA, Aug. 1997, pp. 527-532.

[17] W. C. Gibson, *The Method of Moments in Electromagnetics*. Chapman & Hall/CRC, 2007.

[18] E. M. Purcell and D. J. Morin, *Electricity and Magnetism*, 3rd ed., Cambridge University Press, 2013.

[19] S. Franco, *Design with Operational Amplifiers and Analog Integrated Circuits*, 4th edition. McGraw-Hill Education, 2014.

[20] T. Addabbo, A. Fort, M. Mugnaini, E. Panzardi and V. Vignoli, "A smart measurement system with improved low-frequency response to detect moving charged debris," *IEEE Trans. Instrum. Meas.*, vol. 65, no. 8, pp. 1874-1883, 2016.

[21] N. Nevaranta, J. Parkkinen, T. Lindh, M. Niemelä, O. Pyrhönen and J. Pyrhönen, "Online estimation of linear tooth belt drive system parameters," *IEEE Trans. Ind. Electron.*, vol. 62, no. 11, pp. 7214-7223, 2015.

[22] W. He and S. S. Ge, "Vibration control of a flexible beam with output constraint," *IEEE Trans. Ind. Electron.*, vol. 62, no. 8, pp. 5023-5030, 2015.

[23] A. Kesimli, E. Özkaya and S. M. Bağdatli, "Nonlinear vibrations of spring-supported axially moving string," *Nonlinear Dynam.*, vol. 81, no. 3, pp. 1523-1534, 2015.

[24] S. Chowdhury and R. K. Yedavalli, "Dynamics of belt-pulley-shaft systems," *Mech. Mach. Theory*, vol. 98, pp. 199-215, 2016.

[25] R. A. Sack, "Transverse oscillations in travelling strings," *Br. J. Appl. Phys.*, vol. 5, pp. 224-226, 1953.

[26] W. D. Greason, "Investigation of a test methodology for triboelectrification," *J. Electrostat.*, vol. 49, no. 3-4, pp. 245-256, 2000.

[27] J. B. Gajewski, "Accuracy of cross correlation velocity measurements in two-phase gas–solid flows," *Flow Meas. Instrum.*, vol. 30, pp. 133-137, 2013.

[28] W. Zhang, C. Wang and Y. Wang, "Parameter selection in cross-correlation-based velocimetry using circular electrostatic sensors," *IEEE Trans. Instrum. Meas.*, vol. 59, no. 5, pp. 1268-1275, 2010.

Yonghui Hu received the B.Eng. degree in automation from Beijing Institute of Technology, Beijing, and the Ph.D. degree in dynamics and control from Peking University, Beijing, in 2004 and 2009, respectively.

He was a Post-Doctoral Research Fellow with Beihang University, Beijing, from 2010 to 2012. He is currently an Associate Professor with the School of Control and Computer Engineering, North China Electric Power University, Beijing. His current research interests include measurement of multiphase flow and condition monitoring of mechanical systems.
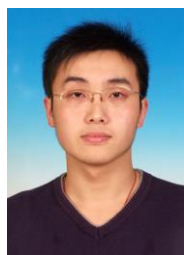
Shuai Zhang received the B.Eng. degree in measurement and control technology and instrumentation from Qingdao Technological University, Shandong, China, in 2011. He is currently pursuing the Ph.D. degree in measurement technology and instrumentation with North China Electric Power University, Beijing, China. His current research interests include sensor design, digital signal processing, and software development.

Yong Yan (M'04–SM'04–F'11) received the B.Eng. and M.Sc. degrees in instrumentation and control engineering from Tsinghua University, Beijing, China, in 1985 and 1988, respectively, and the Ph.D. degree in flow measurement and instrumentation from the University of Teesside, Middlesbrough, U.K., in 1992.

He was an Assistant Lecturer with Tsinghua University in 1988. He joined the University of Teesside, as a Research Assistant, in 1989. He was a Lecturer with the University of Teesside from 1993 to 1996, and then as a Senior Lecturer, a Reader, and a Professor with the University of Greenwich, Chatham, U.K., from 1996 to 2004. He is currently a Professor of Electronic Instrumentation, the Head of the Instrumentation, Control, and Embedded Systems Research Group, and the Director of Research with the School of Engineering and Digital Arts, University of Kent, Canterbury, U.K. He has been a 1000-Talent-Plan Scholar with North China Electric Power University, Beijing, since 2011. His current research interests include multiphase flow measurement, combustion instrumentation, and monitoring and optimization of industrial processes.

Lijuan Wang received the B.Eng. degree in computer science and technology from Qiqihar University, Qiqihar, China, in 2010, and the Ph.D. degree in measurement and automation from North China Electric Power University, Beijing, China, in 2015.

She is currently involved in a post-doctoral research in instrumentation and measurement with North China Electric Power University, Beijing. Her current research interests include electrostatic sensing, flow measurement, and digital signal processing.

Xiangchen Qian received the B.Eng. degree in automation from Tianjin University of Technology, Tianjin, China, in 2004, the M.Sc. degree in automatic meter and device from Tianjin University, Tianjin, in 2007, and the Ph.D. degree in electronic engineering from the University of Kent, Canterbury, U.K., in 2013.

He is currently a Lecturer with the School of Control and Computer Engineering, North China Electric Power University, Beijing, China. His current research interests include multiphase flow measurement techniques, development of instrumentation systems, and digital signal processing.

Lu Yang received the B.Eng. degree in measurement and control technology and instrumentation from North China Electric Power University, Beijing, China, in 2014. He is currently studying for the M.Sc degree in measurement technology and instrumentation with North China Electric Power University. His current research interests include electrostatic sensing, vibration measurement, and digital signal processing.